Cleaner Engineering and Technology 27 (2025) 101042

Contents lists available at ScienceDirect

Cleaner Engineering and Technology

journal homepage: www.sciencedirect.com/journal/cleaner-engineering-and-technology

Concurrent removal of *benzene, toluene, and P-nitrophenol* from water using dielectric barrier discharge plasma

Vaishnavi Gaude Agadyekar [a,1], Eshita Kakodkar [a,1], Delicia A. Barretto [a], Ruggero Barni [b], Claudia Riccardi [b], Nitesh Joshi [a,b,*]

[a] School of Chemical Sciences, Goa University, Taleigao Plateau, 403206, Goa, India
[b] Dipartimento di Fisica G. Occhialini, Università degli Studi di Milano-Bicocca, Piazza della Scienza 3, I-20126, Milano, Italy

ARTICLE INFO

Keywords:
P-Nitrophenol
Dielectric barrier discharge
Degradation
Benzene
Toluene
Escherichia coli

ABSTRACT

Water bodies are contaminated with organic and inorganic waste, making them unsuitable for consumption. This study, for the first time, carries out the degradation of a single pollutant, *p*-nitrophenol (PNP), as well as a mixture of pollutants (*benzene, toluene,* and *PNP*) in a single go using a dielectric barrier discharge (DBD) plasma reactor. The effects of plasma power and treatment time on pollutant degradation were systematically analysed. For *PNP,* only 70 ± 5 % degradation was achieved at optimal conditions (18 W power, 2 min) with an energy efficiency of 1.57 mg/kWh at 10 ppm of initial concentration. The increased power levels diminish performance due to quenching effects caused by microfilament interactions with the reactor walls. Hydroxyl radical, superoxide radical, hydrogen peroxide, ozone, nitrate, and nitrite species were quantified to understand degradation mechanisms. The degradation of a mixture of pollutants is also demonstrated in a single go with 55 % and 0.73 gCOD/kWh COD degradation and energy yield. The practicality of plasma-treated water was tested by biochemical oxygen demand (BOD), seed germination, and microbial decontamination study (using *Escherichia coli*). It is demonstrated that compared to polluted water, plasma-treated water exhibited reduced BOD levels, which reduces its harmful effects on daily usage. The reduced toxicity of water also enhanced germination compared to polluted water. The plasma treatment also impedes the growth of *Escherichia coli,* even causing its complete inhibition. These results highlight the potential of DBD plasma technology as a promising tool for sewage/contaminated water samples.

1. Introduction

Over the years, hazardous pollutants have severely depleted water quality. The primary sources of pollutants are industrial effluents, pesticides, and fertilizers from agricultural runoff, as well as sewage and urban runoff. The organic and inorganic pollutants in such polluted waters could lead to mild to severe health issues, from mild skin allergies to cancerous growth in the body. Thus, these polluted water bodies are rendered useless, and when mixed with other water bodies, they become unfit for human usage. *P*-nitrophenol (PNP) is a type of organic pollutant present in effluents of industrial bodies. The PNP is used in drug manufacturing, fungicides, insecticides, dye production, and leather darkening (Kulkarni, M. & Chaudhari, A., 2007). PNP also finds its application in the manufacture of parathion, *N*-acetyl-*p*-aminophenol (acetaminophen), dyestuffs, and as a leather treatment agent (Chemical Marketing Reporter, 1990; Lewis, 2016). The varied use of PNP in industrial sectors often leads to the leaching of this chemical into the environment, especially to water bodies through various waste streams. Graedel and McGill. (1986) have documented that PNP is a product of the photooxidation of nitrobenzene in the air. Nojima et al. (1983) identified it can also be formed in the air by a process called nitration involving the reaction of aromatic hydrocarbons such as benzene, toluene, and phenanthrene with nitric oxide. It is also emitted from vehicular exhaust from both gasoline and diesel engines (Tremp et al., 1993). It is a degradation product of parathion (Howard et al., 2017) and an impurity in the parathion formulation Thiophens and, therefore, is released during the insecticide application (Archer, 1975). PNP has been listed as one of the 129 priority toxic pollutants by the U.S. Environmental Protection Agency (Keith and Telliard, 1979). Many technologies are adopted to remove PNP and other pollutants from water bodies. For

* Corresponding author. School of Chemical Sciences, Goa University, Taleigao Plateau 403206, Goa, India.
E-mail addresses: Nitesh.joshi@unimib.it, nitesh.joshi@unigoa.ac.in (N. Joshi).
[1] Equal contribution.

https://doi.org/10.1016/j.clet.2025.101042
Received 25 March 2025; Received in revised form 9 June 2025; Accepted 25 June 2025
Available online 28 June 2025

instance, ozonolysis (Gu et al., 2008), UV photocatalysis (Othman et al., 2019), Fenton-based conversions (Zeng et al., 2019), adsorption (Yao et al., 2014), and others. These techniques are called advanced oxidation techniques as they rely on the oxidation of contaminants *via* interaction with reactive species, *viz* hydroxyl radical ($^{\bullet}OH$), superoxide radical ($^{\bullet}O_2^-$), ozone (O_3), hydrogen peroxide(H_2O_2), and others. Non-thermal plasma (NTP)- based processes are an effective AOP (advanced oxidative process) as they can create reactive species easily, efficiently, and quickly, unlike other techniques, which are laggy and time-consuming. Additionally, one can easily switch on and off a process during a longer cycling process without affecting the operationality of the process. Lastly, reactive species concentration could be varied by just switching power injected. This results in the usage of NTP in wide areas of research. For instance, the mitigation of greenhouse gases using NTP is well documented in the review by Joshi et al. (2022) and material synthesis and modification for greenhouse gases mitigation (Joshi and Loganathan, 2024). The gas phase catalytic application, namely conversion of CO2 (Joshi and Loganathan, 2023) and propane decomposition (Piferi and Riccardi, 2022), are also well documented. The non-thermal plasma finds its application in air sanitation by evaluating electrical parameters of NTP (Piferi et al., 2021) and generating and modelling species evolution by 0D kinetic modelling for end usage towards air sanitization (Pierotti et al., 2023). The NTP-based plasma techniques are of prime importance as complete mineralization can be achieved without needing an external catalyst, which can reduce the overall cost of the technique.

A handful of literature reports dealing with removing PNP from wastewater effluent using plasma are available. For instance, pulse discharge was engaged by Wang et al. (2015) for degradation of PNP from soil sediments. The authors attained 92.8 % removal efficiency (200 ppm as the initial concentration) at 60 min plasma with 17 kV of applied potential. Li et al. (2015) have reported the removal of PNP from the soil with a removal efficiency of 73 % at a power of 42.2 W with an initial concentration of 200 ppm. Shang et al. (2019) employed oxidant per sulphate (SO_4^-) in combination with DBD plasma to degrade PNP. With 5 ppm as the initial concentration of PNP, the author attained 63.7 % degradation efficiency at 6.37 W of input power. The plasma treatment time was 50 min with a persulphate (PS) dosage of 0.25 mM. Interestingly, when Fe^{+2} was added along with 0.25 mM per sulphate, the conversion rose to 81.1 %. It was attributed to the synergistic interaction of Fe/PS, which leads to the production of $^{\bullet}OH$ and SO_4^-, and to enhanced degradation. In another work, Shang et al. (2017) reported the decomposition of PNP using peroxydisulphate (PDS) by gas-liquid pulsed discharge plasma. The authors achieved 90 % degradation efficiency with a PDS: PNP molar ratio of 80:1 with ~13 W input power. Chen et al. (2019) have used a plasma jet to decompose PNP in water. The authors attained 55 % conversion at 43 mJ of plasma discharge energy and a treatment time of 5 min. Long et al. (2021) used modified electrode $CoFe_2O_4$/MWNTs/sponge to decompose PNP and attained 98.5 % conversion with an initial concentration of 10 ppm of PNP at an applied voltage of 30 V and a plasma treatment time of 40 min. Gu et al. (2008) have employed plasma-activated charcoal for adsorption and removal of PNP using an O_3 dosage of 2.53 g/h. The plasma treatment increases PNP adsorption capacity from 254.9 to 304.0 mg/g for 1000-ppm initial concentration. Later, the adsorbed PNP was decomposed by ozonolysis, and ~75 % conversion was achieved. Wang et al. (2012) used a multi-tube parallel surface discharge plasma reactor for the decomposition of 80 ppm of COD (~40 ppm of PNP) of initial concentration. The authors attained 97 % conversion using 30 kV of applied voltage and 3 h of treatment time. Ferhat et al. (2017) designed a novel gliding arc discharge reactor to exclude the direct contact between the plasma plume and the liquid, which allowed 90 % removal of PNP after 120 min. About 15 % conversion of PNP was achieved with an initial concentration of 100 ppm by peak voltage 110 V and treatment time of >30 min using a DBD reactor by Wang et al. (2020). Zhao et al. (2021) developed an electrodeless high-flow microwave atmospheric plasma jet for fast degradation of PNP from water. The authors achieved a remarkable 100 % removal efficiency of 100 ppm of PNP in 12 min, with a total organic carbon (TOC)removal efficiency of 57.6 %. This was attributed to a high cross-section area of plasma, which creates surplus $^{\bullet}OH$ radical species, leading to efficient degradation. Zhao et al. (2022) carried out the simultaneous removal of PNP and reduced toxic Cr^{+6} from water using microwave atmospheric pressure plasma. Mere 15 min of treatment time led to 97.5 and 93.6 % removal efficiency of Cr^{+6} and PNP, respectively, with the total organic carbon in the sample reaching 30.2 %. Argon plasma and air-mixed argon plasma jets are utilized for the degradation of PNP by Acharya et al. (2024). Out of the two plasma jets, the air-mixed Argon jet with air outperforms the pure Argon plasma jet. The PNP degradation was 97.2 %, and a maximum energy efficiency of 57.3 $gkW^{-1}h^{-1}$ for a 6-min treatment time at 100 ppm initial concentration. Corona discharge needle-to-plate type coupled with graphene-ZnO nanoparticles was used by Guo et al. (2022). The authors achieved PNP degradation of 68.5 % with plasma alone, 80.2 % with ZnO catalyst addition, and 97.6 % with graphene (6 %)-ZnO nanocomposites under the same catalyst loading amount with a plasma peak voltage of 20 kV, frequency of 50 Hz, air flow rate 4 L per minute and PNP concentration of 30 ppm. Farzinfar and Qaderi (2022) have degraded PNP by utilizing a synergistic combination of ZnO photocatalyst with DBD plasma. The authors obtained PNP degradation of 13 % in ZnO using 15 W UV light, 68 % PNP degradation in DBD alone, and 93.6 % PNP degradation by combining ZnO photocatalyst with DBD plasma operated at 13 kV of applied voltage, ZnO concentration 250 ppm, and plasma treatment time of 30 min with an initial PNP concentration of 15 ppm. Khourshidi et al. (2024) performed PNP degradation using the circulation of O_3 generated during DBD plasma. DBD-O_3 increases the PNP degradation efficiency from 57.4 to 94.4 % with improved energy yield by 130 % from 0.52 to 1.18 g $kW^{-1}h^{-1}$. The authors attribute the enhancement in PNP degradation to an increase in long-lived and short-lived reactive species (ROS) in the DBD-O_3 system by the O_3 circulation. Although extensive literature is available, most studies either rely on employing high plasma power or longer treatment time, which decreases the energy efficiency of the process. Thus, the ideal methodology would operate in an energy-saving mode without adding external substrates whose separation again adds up the cost of the technique.

In real life, a polluted water body consists of multiple organic and inorganic pollutants, pathogens, sediments, and even microplastic residues (Mhapsekar et al., 2025). Most studies deal with removing a single pollutant rather than a complex mixture, as multiple pollutant degradation is tedious task. Apart from PNP pollutants from crude oil and petroleum derivatives, they also contribute to water contamination. Crude oil are the primary sources of BTEX (benzene (B), toluene (T), ethylbenzene (E), and paraxylene (X)). The production and usage of BTEX have increased over the years due to the expansion of the petrochemical and petroleum industries (Bustillo-Lecompte et al., 2018). Benzene and toluene are common volatile organic compounds (VOCs), often in polluted air and water. They mainly come from petrochemical industries, gasoline leaks, industrial solvents, and incomplete combustion. The International Agency for Research on Cancer (IARC) classifies benzene as a Group 1 carcinogen, which presents severe health risks even with low exposure, such as leading to hematotoxicity and a greater likelihood of leukemia (Loprieno, 1975). Benzene, one of the BTEX compounds, is now among the most common chemicals in the world. The large-scale discharge of benzene poses a significant threat to public health. Benzene and toluene are the most hazardous of all the BTEX chemicals due to their ability to enter the human body rapidly and disseminate throughout it. Although toluene is less acutely toxic, it can cause neurotoxic effects and developmental problems with long-term exposure (El-Hagrasy et al., 2025).Prolonged exposure to BTEX can adversely affect the central nervous system, respiratory functions, and skin health (Anjum et al., 2019).

Both substances persist in aquatic environments due to their low

solubility and high volatility, which hinder biodegradation during regular aerobic or anaerobic treatment processes (Masumoto et al., 2014). Their stable aromatic ring structures make them resistant to microbial degradation, often requiring more advanced treatment techniques (Lhotský et al., 2017).

When present alongside phenolic compounds like p-nitrophenol (PNP), benzene and toluene may experience co-degradation through advanced oxidation or plasma-induced processes. This occurs *via* non-selective radical mechanisms, such as $^{\bullet}OH$ attacks, which can simultaneously target several aromatic structures. Investigating benzene, toluene, and PNP co-degradation offers a more accurate perspective on mixed wastewater streams and can uncover potential synergistic or inhibitory interactions among pollutants during treatment.

In this study, we demonstrate for the first time the potential of DBD plasma to degrade a single pollutant (*PNP*) and multiple pollutants (*benzene, toluene, and PNP*) and model pathogenic bacteria *E. coli* in a single go using a DBD reactor. We have evaluated the influence of plasma power, treatment time, and a concentration-dependent study on the decomposition of the single pollutant PNP. The optimized parameters for plasma power and treatment time were utilized to degrade multiple pollutants and microbial growth inhibition using *E. coli* as a bacterial strain in a single go. Multiple pollutant degradation was monitored through COD (chemical oxygen demand) analysis. BOD (biochemical oxygen demand) was also carried out to study the decomposition of organic matter in a plasma-treated water sample. The toxicity study of the water sample was also conducted to understand the real-life impact of the treated water on seed germination using wheat seeds and bacterial growth inhibition using *E.coli* as an indicator organism for water quality. The study evaluates the practicality of the setup, thus paving the way for further research upscaling.

2. Materials and methods

TCI and Merk Industries PVT LTD supplied the chemicals used in the study: P-Nitrophenol (PNP) (98 %) assay, Potassium dichromate ($K_2Cr_2O_7$) (99 %) assay, Sulfuric acid (H_2SO_4) (98 %) assay, silver sulphate ($AgSO_4$) (98 %) assay, Mercury sulphate ($HgSO_4$) (99 %) assay, ferrous ammonium sulphate (FAS) (98.5 %) assay, ferroin indicator, Manganese sulphate ($Mn_SO_4{\cdot}2H_2O$) (98 %) assay, Potassium Iodide (KI) (99 %) assay, Potassium Hydroxide (KOH) (85 %) assay, Sodium thiosulphate ($Na_2S_2O_3$) (99.5 %) assay, Starch indicator, Titanium sulphate (~15 wt %), H_2O_2 (30 %) assay, Terephthalic acid (>98.0 %), Nitro blue tetrazolium salt (NBT) (98.0 %), ethanol (99.9 %) assay, isopropanol (99.8 %) assay, methanol (99.8 %) assay, sodium Nitrite (98 %) assay, concentrated hydrochloric acid (36 %) assay, sulphanilamide (98 %) assay, N-(1-naphthyl)ethylene diamine·2HCl (99 %) assay, and zinc dust.

2.1. Plasma reactor construction

The schematic of the plasma reactor is presented in Fig. 1. The reactor is constructed from borosilicate glass. An aluminium tape is applied at the bottom of the reactor vessel, serving as a ground electrode with a diameter of 30 mm. The electrode arrays are made using stainless steel tubes with an outer diameter of 0.6 mm. These 10 electrodes are arranged cylindrically, with a 5 mm distance between each electrode. The electrodes are electrically connected *via* aluminium tape to an opening in the gas inlet. The gas inlet flows at a rate of 0.1 L per minute, pumped by an air pump. The flow passes through the array of electrodes. The plasma is generated using an HV transformer, as shown in Fig. 1. The dimensions of the transformer are 205 × 120 × 90 mm. The transformer operates at 240 V of AC voltage and steps up to a maximum of 6 kV. It can provide a peak output power of 400 W, achieved with a fixed frequency of 16 kHz and a variable output voltage ranging from 0 to 6 kV. The real-time power the transformer consumes from the electrical socket is measured using the Quick Sense Energy Meter D69-0258 model. A volume of 5 mL of batch solution was used for water treatment, maintaining a distance of 10 mm between the electrodes and the water. A detailed picture of the plasma reactor and plasma generation is presented in Figs. S1 and S2 **ESI†**. For the experiment, 5 mL of 10 ppm PNP solution was used unless otherwise mentioned. The solution was prepared using distilled water with pH and 6.8 and 11.2 μS/cm^2 conductivity, respectively.

2.2. Analysis of reactive species produced in plasma

2.2.1. Quantification of O_3

The gas flow from the plasma reactor was bubbled through the solution in a conical flask for 2 min after plasma ignition. The solution in the conical flask comprised 10 mL of 2 M HCl, 10 mL of 10 % KI, and 5 mL of a phosphate buffer with a pH of 7. During the gas bubbling, the solution turned yellow-brown as iodine was liberated. Subsequently, the solution was titrated with a standardized 0.1 M $Na_2S_2O_3$ solution and 1 mL of starch solution as an indicator. When the endpoint was reached, it was marked by a colour change from blue to colourless. The amount of O_3 present in the reaction mixture was estimated using Equation 1

$$\text{Normalized } O_3\left(\frac{\text{ppm}}{\text{min}}\right) = \frac{24 * V_{Thio} * N_{Thio} * 1000}{120} \qquad \text{Equation 1}$$

In the above equation, V_{Thio} and N_{Thio} are the volume and normality of the thiosulphate solution, respectively.

2.2.2. Determination of H_2O_2

The amount of H_2O_2 (long-lived species) generated during the plasma discharge process was measured using the titanium sulphate

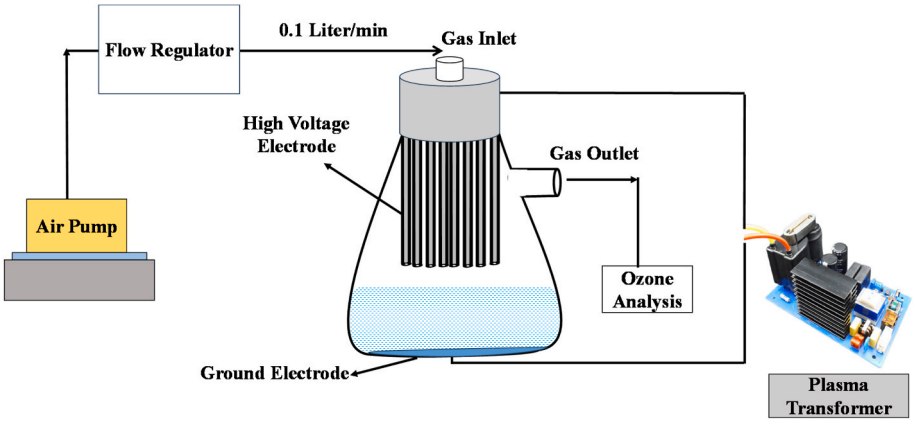

Fig. 1. Schematic of the plasma reactor.

method by (Chandana et al., 2022; Meiyazhagan et al., 2020). Titanium sulphate reacts with H_2O_2 to create per titanic acid (yellow colour complex), which absorbs at 420 nm (Chandana and Subrahmanyam, 2017; Meiyazhagan et al., 2020; Eisenberg, 1943). The maximal absorbance of pertitanic acid at 420 nm was measured using a UV–vis spectrophotometer (UV-2450, Shimadzu, Japan). To estimate H_2O_2 in plasma, a 0.1 M titanium sulphate solution was prepared, with 2 mL of titanium sulphate added to 2 mL of plasma-treated water for analysis. For H_2O_2 calibration, various concentrations of H_2O_2 were introduced to the 0.1 M titanium sulphate solution, during which the corresponding increase in peak absorbance was observed and presented in Fig. S5 **ESI†**.

2.2.3. Estimation of $^{\bullet}O_2^-$ anion radical

The analytical method described by Goto et al. (2004) was used to estimate the $^{\bullet}O_2^-$ ion using nitroblue tetrazolium salt (NBT). The superoxide radical in a water-based solution is unstable; therefore, NBT was used to react swiftly with $^{\bullet}O_2^-$. NBT reacts with $^{\bullet}O_2^-$ radicals to form a stable compound, formazan, which serves as the basis of quantification. During the study, a solution of NBT was prepared by dissolving 42 mg of NBT in 100 mL of Milli-Q water and 10 % ethanol. A volume of 3 mL of the NBT solution was utilized in each run. To ensure the scavenging of $^{\bullet}OH$ radicals produced, 0.1 mM of isopropanol was added. Additionally, samples were regularly withdrawn from the reactor and mixed with 2 mL of methanol to dissolve the formazan completely. The presence of formazan is identified by strong absorption at 530 nm using a UV–vis spectrophotometer (UV-2450, Shimadzu Japan).

2.2.4. Quantification of $^{\bullet}OH$ radical

The $OH^{\bullet}$ radicals are significant oxidant species in ROS and are essential in the degradation process (Wang et al., 2016). Consequently, the production of $^{\bullet}OH$ as a function of plasma power and treatment time was analysed to understand the degradation process. For this purpose, 3 mL of 0.05 mM terephthalic acid solution was prepared in water by adding sodium hydroxide to enhance solubility (NaTA). The NaTA solution (3 mL) was treated under various plasma discharge conditions. When plasma interacts with the NaTA liquid, $^{\bullet}OH$ radicals are generated. This reaction mixture yields hydroxy terephthalic acid (HTA), which exhibits a strong emission peak at 425 nm when excited with a wavelength of 315 nm. The Carry Eclipse fluorescence spectrophotometer was employed to obtain the emission spectrum. The reaction yield of the NaTA molecule scavenging $^{\bullet}OH$ radicals was assumed to be 35 % (Sahni and Locke, 2006).

2.2.5. Determination of COD (chemical oxygen demand) and BOD (biological oxygen demand)

The COD analysis was performed according to the procedure provided by the US EPA method #410.3, Stort No. 00340, using the titration method. In brief, 10 mL of sample solution, 10 mg of $HgSO_4$, and 5 mL of concentrated H_2SO_4 were added to the sample. The solution was swirled until the $HgSO_4$ dissolved completely. Following this step, 25 mL of 0.25 N $K_2Cr_2O_7$ solution was added. Then, 70 mL of sulfuric acid-silver sulphate was introduced with continuous swirling until thoroughly mixed, and the mixture was refluxed at 90 °C for 2 h. After the solutions cooled to room temperature, they were titrated against the FAS solution using a ferroin indicator.

Winkler's technique was employed to assess the BOD of the samples (APHA, 2017). To ascertain dissolved oxygen after plasma treatment, 5 mL of the plasma-treated solution at various discharge powers and durations was filled into a 10 mL bottle to the neck and sealed alongside a blank solution (untreated solution). The bottles were incubated for 7 days with a blank. After incubation, 1 mL of $MgSO_4$ and 1 mL of alkali iodide solution were added. The resulting brown precipitate was allowed to settle, and then 1 mL of concentrated H_2SO_4 was introduced to dissolve the precipitate, yielding a pale-yellow solution. This solution was titrated against a 0.001 M $Na_2S_2O_3$ solution with a starch indicator. From this, the amount of dissolved oxygen was calculated. The same procedure was followed to determine the D0 (day one) and the incubated samples after 7 days (D7) by subtracting the dissolved oxygen values from D0 and D7 to obtain the BOD for each sample solution.

$$\text{BOD}\left(\frac{\text{mg}}{\text{L}}\right) = \frac{(\text{D0}_{\text{BOD}} - \text{D7}_{\text{BOD}})*8*\text{N}_{\text{Thio}}*1000}{\text{Volume of solution pipetted out (mL)}} \quad \text{Equation 2}$$

The PNP concentration as a function of plasma power and treatment time is analysed using a UV–vis Spectrophotometer (UV-2450, Shimadzu Japan) and COD analysis by titration. The % degradation of PNP is calculated using Equation (3).

$$\%\ \text{PNP degrdation} = \left[\frac{C_i - C_f}{C_0}\right] \times 100 \quad \text{Equation 3}$$

Herein C_i and C_f are the initial concentration of PNP at time zero (initial concentration) and time t (mg/L), respectively. The energy yield was calculated using Equation (4).

$$\text{Energy yield}\left(\frac{\text{g}}{\text{KWh}}\right) = \frac{(\text{C}_\text{i} \times \text{DE} \times \text{V}) \times 100}{\text{P} \times \text{t}} \quad \text{Equation 4}$$

In Equation (4) C_i is the initial concentration of PNP (g/L), DE is degradation efficiency given in (%), V is the volume of solution used in the study (Liters), P is power (kW), and t is time (hours).

2.2.6. Phytotoxicity and bacterial toxicity

The phytotoxicity and bactericidal toxicity of plasma-treated and untreated solutions were examined to understand the practicality of DBD plasma-treated samples.

2.2.7. Phytotoxicity assessment

The phytotoxicity assessment used wheat seeds (*Triticum aestivum*) purchased from Vibrex company, India. For each test, a maximum of three samples were set up. Briefly, in each Petri dish, 10 seeds were placed on cotton soaked in the plasma-treated sample, and an untreated sample was added alongside distilled water as a control. The germination rate and seedling growth were monitored for at least 5 days.

2.2.8. Bactericidal effect of plasma

The time-dependent and power-dependent bactericidal efficiency of plasma was evaluated against the indicator coliform bacteria *Escherichia coli* (ATCC® 11775™), as reported by Lunov et al. (2016). The experiments were conducted under sterile conditions. Bacterial cells were inoculated in sterile nutrient broth and incubated at 37 °C for 18 h. A cell pellet was obtained by centrifuging the inoculated broth at 6000 rpm for 10 min. The pellet was washed twice with sterile phosphate-buffered saline (PBS, pH 7.2). A 1.5 × 108 cells/mL bacterial suspension was prepared according to the 0.5 McFarland turbidity standard. This suspension was diluted to achieve a 5×10^5 CFU/mL cell density in nutrient broth for each treated and untreated culture flask. *E. coli* cells in the inoculated flasks underwent subsequent plasma treatment. The plasma treatment experiments were conducted in two sets. In the first set, the plasma power was kept constant at 22 W, while the time intervals were varied to 0, 1, 2, 3, 4, 5, and 10 min. In the second set of experiments, the treatment time was maintained at 2 min, and plasma power was varied from 18, 26, 30, and 40 W. A 100 μL cell suspension sample from treated and untreated (control) flasks was swab inoculated onto the appropriately labelled sterile nutrient agar Petri dishes. The inoculated petri dishes were then incubated at 37 °C for 24 h. The experiments were performed in triplicate, and the results were expressed as mean ± SD. The percentage of growth inhibition of *E. coli* cells was calculated using the formula as shown in Equation (5).

$$\text{Growth inhibition}\ (\%) = \left[\frac{(\text{A} - \text{B})}{\text{A}}\right] \times 100 \quad \text{Equation 5}$$

where A = Growth of control or untreated cells in CFU/mL, B = Growth of treated cells in CFU/mL.

3. Results and discussion

Fig. 2 depicts the PNP degradation and energy yield as a function of input power. The general overview of the graph indicates that PNP degradation and energy yield decrease as plasma power increases. The energy yield relies directly on PNP degradation and is inversely proportional to input power; hence, as degradation declines with rising power, the energy yield correspondingly diminishes. At 18 W of input power, a PNP degradation of 70 % and an energy yield of 1.57 mg/kWh can be achieved. Increasing power to 22 W reduces PNP degradation and energy yield to 65 % and 1.22 mg/kWh, respectively. Further increase in power reduces PNP degradation from 60 % to 55 % at 26 and 32 W, respectively. The energy yield decreases from 0.9 to 0.56 mg/kWh. This observed trend may be attributed to the following factors: 1) The decrease in the concentration of reactive species (reactive oxygen and nitrogen species) generated in-situ, which facilitates the degradation of PNP, 2) The overall power consumed is not directed towards degradation but is instead used to increase the thermal temperature of the reactor.

Upon igniting plasma in the gas phase, primary, long-lived NO, NO_2, and O_3 species are generated. The detailed mechanism of species production is presented in Table 1. The production of O_3 is presented in R8. The reaction proceeds *via* the reaction of singlet oxygen radical with oxygen gas. Furthermore, due to the immense reactivity of the oxygen radical, it reacts with N_2 gas to produce NO, as presented in R6. The NO gas produced can be intrinsically converted to NO_2 *via* the reaction shown in R9. Apart from primary long-lived species, the long-lived species react to produce secondary short-lived species with high oxidation potential. Species, namely $^{\bullet}OH$, H_2O_2, $^{\bullet}O$, $HO_2^{\bullet}$, and others are produced by various reactions as presented in Table 1. In the presence of water, the detailed reactions of species are given from R10-R20. The production of H_2O_2, $^{\bullet}O_2$- and $HO_2^{\bullet}$ is possible in water, as shown by R10, R20, R11 and R12, respectively. Out of reactive oxygen species, the oxidation potential for $^{\bullet}OH$ is highest, which is 2.8 eV > $^{\bullet}O_2^-$, 2.42 eV > O_3 2.1 eV > H_2O_2 1.7 eV (Mcguire and Jakhete, 2012). Thus, $^{\bullet}$OH species quantification becomes essential, and their role in PNP degradation needs to be evaluated. The ROS species quantified in the solution are presented in Figs. 3 and 4.

Fig. 3 (a) illustrates the effect of plasma power on $^{\bullet}OH$ radical species produced in plasma. As the plasma input power increases from 18 to 40 W, the $^{\bullet}OH$ radical species decreases 1.3-fold. This observed trend is attributed to species quenching due to a rise in water temperature and a decrease in pH. The pH of the solution falls to 2.3, and the temperature rises to 50 °C for 22 W of plasma power, compared to the initial pH of 6.8 and temperature of 30 °C, as shown in Fig. S3 ESI†.

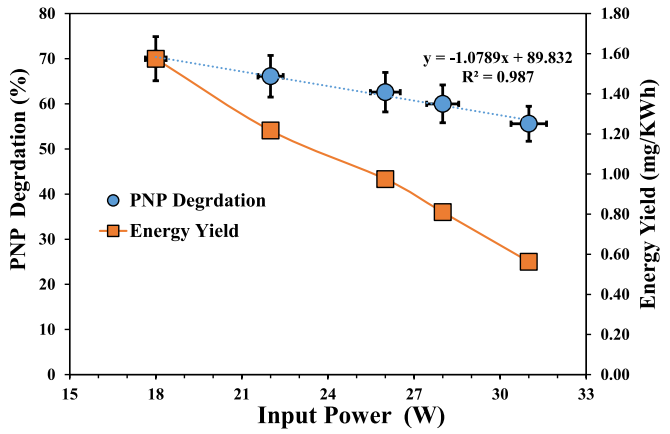

Fig. 2. The degradation profile of PNP as a function of plasma power at a fixed treatment time of 2 min. The error bars indicate standard deviation with sample size n = 3.

Table 1
List of chemical reactions which occur in plasma.

		Reactions	Reference
Gas phase	R1	$e + H_2O \rightarrow e + H^{\bullet} + {}^{\bullet}OH$	(Yukinori et al., 2012; Penetrante et al., 1997; Chen et al., 2014)
	R2	$e + O_2 \rightarrow e + 2(O^{\bullet})$ (1D)	
	R3	$H_2O + 2(O^{\bullet})$ (1D) $\rightarrow 2^{\bullet}OH$	
	R4	$e + N_2 \rightarrow e + N_2^{\bullet}$	
	R5	$N_2^{\bullet} + O_2 \rightarrow e + N_2 + 2(O^{\bullet})$ (1D)	
	R6	$N_2 + (O^{\bullet})$ (1D) $\rightarrow NO + N^{\bullet}$	
	R7	$N^{\bullet} + OH^{\bullet} \rightarrow e + NO + H^{\bullet}$	
	R8	$O^{\bullet} + O_2 + M \rightarrow O_3 + M$	
	R9	$NO^{\bullet} + O_3 \rightarrow NO_2 + O_2$	
In the presence of water	R10	${}^{\bullet}OH + {}^{\bullet}OH \rightarrow H_2O_2$	Oba et al. (2011)
	R11	$O_3 + H_2O \rightarrow HO_2^{\bullet} + O_2$	(Penetrante et al., 1997; Tas et al., 1997; Oba et al., 2011)
	R12	$H^{\bullet} + O_2 + M \rightarrow HO_2^{\bullet} + M$	
	R13	$H^{\bullet} + HO_2^{\bullet} \rightarrow H_2O_2$	
	R14	$H_2O_2 + 2O_3 \rightarrow 2OH^{\bullet} + 3O_2$	(Bedeaux et al., 2011; Golkowski et al., 2012)
	R15	$O_3 + {}^{\bullet}OH \rightarrow 2^{\bullet}OH + 3O_2$	
	R16	$3NO_2 + H_2O \rightarrow 2NO_3^- + 2H^+ + NO$	Chen et al. (2016)
	R17	${}^{\bullet}OH + NO \rightarrow NO_2^- + H^+$	
	R18	$HO_2^{\bullet} + HO_2^{\bullet} \rightarrow H_2O_2$	
	R19	$H_2O_2 \rightarrow H_2O + O_2$	
	R20	${}^{\bullet}OH + HO^- \rightarrow O^{\bullet} + H_2O$	

Similar observations are also made by Parrino et al. (2020), where authors observed $^{\bullet}OH$ concentration decreases with the pH of the solution. Similarly, the temperature effect on $^{\bullet}OH$ radical quenching is evaluated by Koshlyakov et al. (2021). The authors measured reaction rates of $^{\bullet}OH$ radical with trimethyl phosphate in the gas phase. They observed that the rate constant decreases with an increase in reaction temperature, possibly due to the quenching of $^{\bullet}OH$ radical species. Similarly, the effect of plasma treatment time at a fixed plasma input power of 22 W is presented in Fig. 3(b). It is observed that an increase in plasma treatment time results in a decrease in $^{\bullet}OH$ radical concentrations. For instance, as plasma treatment time is extended from 1 to 5 min, the $^{\bullet}OH$ radical concentration decreases fourfold. This trend may be attributed to the extended plasma irradiation time, which leads to significant water heating and a corresponding drop in pH (approximately 60 °C and pH ~2.5). The detailed pH and temperature data are supplied in Fig. S3 ESI†.

Fig. 4 Depicts the $^{\bullet}O_2^-$ species concentration as a function of plasma power and treatment time. The $^{\bullet}O_2^-$ radicals can exist in two forms, *i.e.*, protonated form $HO_2^{\bullet}$ or deprotonated form, i.e., $^{\bullet}O_2^-$. In an acidic medium, it exists in deprotonated form, i.e., $^{\bullet}O_2^-$. Unlike $^{\bullet}OH$ radicals, the $^{\bullet}O_2^-$ radical species concentration increases with plasma power, as seen in Fig. 4 (a). The $^{\bullet}O_2^-$ species concentration increases by 3-fold upon increasing power from 18 to 40 W. Similarly, Fig. 4 (b) represents the $^{\bullet}O_2^-$ species concentration increases with plasma treatment time. During the analysis, no H_2O_2 was produced, and its concentration was below the detection limit of our method Fig. S4–S5 **ESI†**. The radical quenching experiments with scavenger IPA and benzoquinone for scavenging $^{\bullet}OH$ and $^{\bullet}O_2^-$ are carried out and presented in Fig. S6 **ESI†**. It is observed that as scavenger is added for $^{\bullet}OH$, a decrease in pollutant degradation occurs.

Fig. 5 depicts the normalized O_3 concentration as a function of plasma power and time. Fig. 5 (a) shows that the normalized O_3 concentration grows with increased plasma input power. At 18 W, 100 ± 10 ppm O_3 was produced, rising to 160 ± 10 ppm O_3 at 40 W input power. The surge in O_3 concentration with an increase in plasma power is

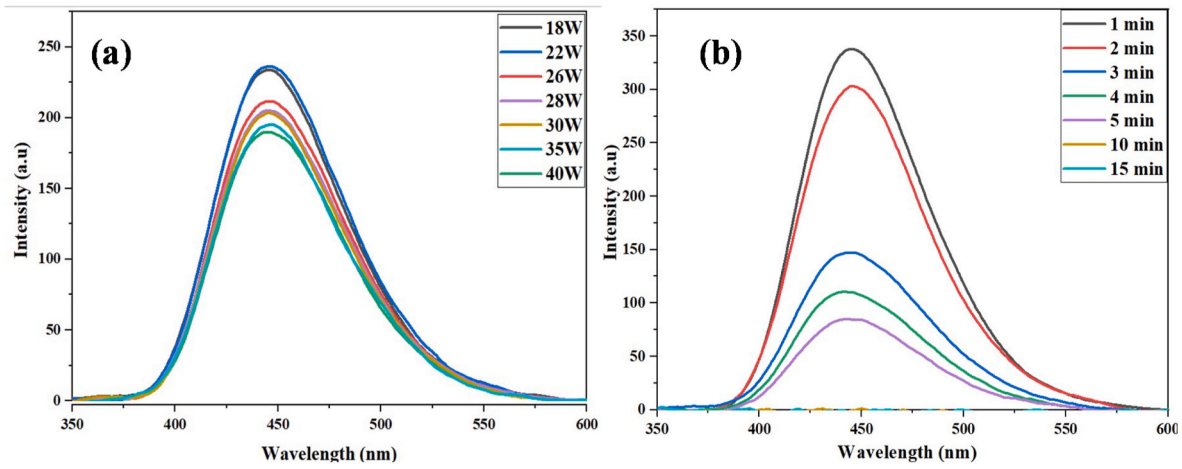

Fig. 3. $^{\bullet}$OH radical quantification (a) as a function of plasma input power at a fixed treatment time of 2 min and (b) as a function of time at a fixed plasma power of 22 W.

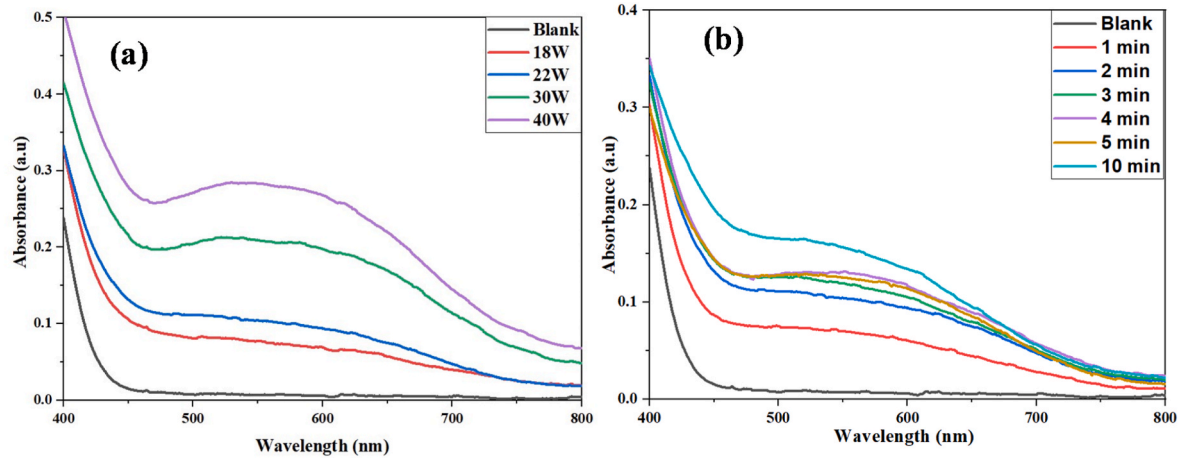

Fig. 4. $^{\bullet}O_2^-$ species quantification (a) as a function of plasma input power at a fixed treatment time of 2 min and (b) as a function of time at a fixed plasma power of 22 W.

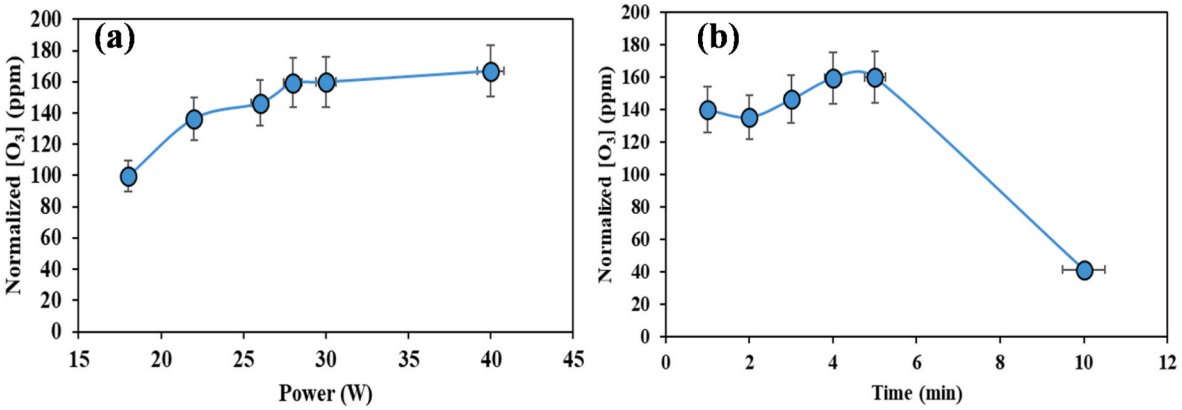

Fig. 5. O_3 species quantification (a) as a function of plasma input power at a fixed treatment time of 2 min and (b) as a function of time at a fixed plasma power of 22 W. The error bars indicate standard deviation with sample size n = 3.

attributed to the rise in micro discharges in plasma reactor volume Fig. S2 **ESI†**. This increase in the number of discharges increases the interaction of plasma streamers with oxygen molecules to create nascent oxygen species, which then react with oxygen molecules to lead to O_3 production, as depicted in R8 Table 1. Fig. 5(b) represents the O_3 produced as a function of plasma treatment time at a fixed plasma power of 22 W. The O_3 produced increases from 140 ± 10 ppm O_3 at 1 min treatment to 160 ± 10 ppm O_3 for 5 min treatment. This could be because the number of micro-discharges at a fixed power might remain the same while the number of O_2 molecules interacting within the

plasma volume increases. However, the difference is negligible, as the rise in reactor temperature leads to the decomposition of the O_3 produced. Extending the plasma treatment time to 10 min reduces the O_3 generated to 40 ppm. This reduction may be due to the heating of the reactor volume, which decreases the O_3 because of its decomposition.

Fig. 6 depicts the impact of plasma treatment time on PNP degradation at a fixed input power of 22 W and corresponding energy yield. A maximum of 83 % degradation is achieved at plasma treatment time <3 min. As the treatment time increases from 3 to 7 min, the degradation efficiency decreases from 83 to 70 %. Similarly, the energy yield decreases as treatment time increases from 3 to 7 min from 1.7 to 1.29 mg/kWh. This is because, as shown in Equation (4), the energy yield decreases with an increase in time and decreases with an increase in degradation. The further increase in treatment time to 15 min leads to 50 % degradation. This is attributed to the lower concentration of reactive species produced and sustained in plasma volume. Prolonged plasma exposure (over 3 min) reduces degradation efficiency due to two main factors. Firstly, prolonged operation increases the thermal load, heating the reactor and promoting the decomposition of short-lived radicals like $^{\bullet}OH$, indicated by solution temperature rise and pH drop (Fig. S3 **ESI†**). Secondly, accumulating intermediate products, like quinones and low molecular weight organic acids, may scavenge active species and compete for oxidation, creating a complex reaction environment that slows the degradation rate of the parent pollutant. Therefore, shorter treatment cycles may better maintain optimal radical activity and degradation efficiency.

3.1. Understanding the impact of concentration on PNP degradation

Fig. 7 depicts the effect of PNP concentration on its degradation at 22 W of input power and 2 min of plasma treatment time. As seen in Fig. 7, at concentrations <15 ppm, a maximum degradation of <95 % is observed. The further increase in PNP concentration decreases the degradation of PNP. The degradation of PNP displays excellent linearity with an R^2 value of 0.91. The decrease in degradation may be linked to the limited amount of RONS species produced in water, which is inadequate to cause complete degradation. Thus, as the concentration of PNP rises, the degradation efficiency declines. The increase in PNP concentration reduces the conversion of PNP. However, the energy yield rises with an increase in concentration. This suggests that even high concentrations of PNP in water can be effectively degraded with plasma. Since the $^{\bullet}OH$ possesses the highest oxidation potential and a very short lifetime, it could dominate the degradation of PNP. Fig. 8 depicts the plausible degradation mechanism of PNP using $^{\bullet}OH$.

The degradation pathway illustrated in Fig. 8 is proposed based on

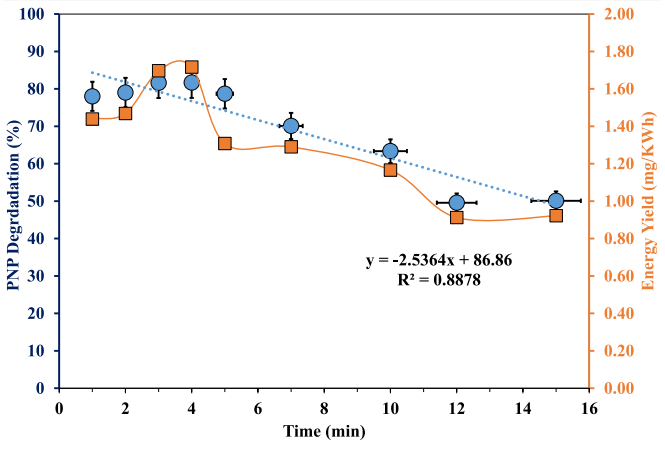

Fig. 6. Effect of PNP degradation as a function of plasma treatment time at fixed power of 22 W. The error bars indicate standard deviation with sample size n = 3.

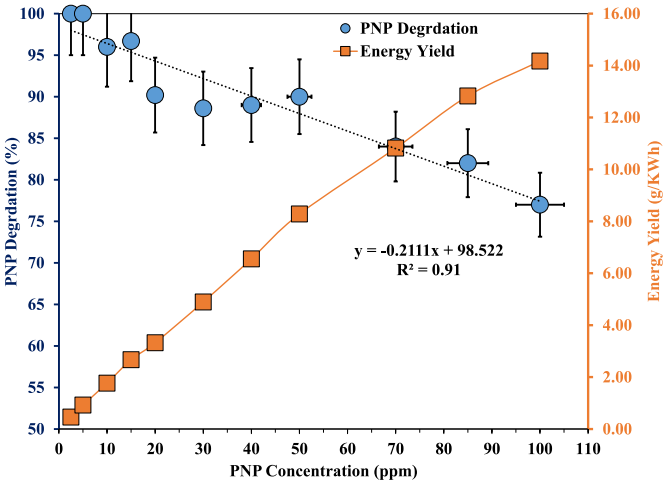

Fig. 7. Effect of PNP concentration on degradation of PNP at fixed input power and treatment time of 22 W and 2 min time, respectively. The error bars indicate standard deviation with sample size n = 3.

the literature. It is primarily driven by $^{\bullet}OH$ radicals' activity, which was supported by quenching experiments conducted in this study (Fig. S6 **ESI†**). However, as intermediate degradation products were not directly identified in our experiments, the mechanism remains hypothetical. Future studies will focus on validating this pathway through detailed characterization of intermediates using techniques such as LC-MS or GC-MS. The degradation of organic pollutants in plasma-treated systems is driven by generating a complex mixture of reactive oxygen and nitrogen species (RONS), each playing a distinct yet interconnected role in the oxidation process. While individual species such as $^{\bullet}OH$ radicals, $^{\bullet}O_2^-$ radicals, and O_3 have been quantified and discussed separately, it is the interplay and synergy among them that underpin the overall degradation efficiency.

Due to their exceptionally high oxidation potential (2.8 eV), $^{\bullet}OH$ radicals are the primary agents for the initial attack on pollutants like PNP through hydroxylation. This leads to ring opening and the formation of intermediate products such as benzoquinone and hydroxyquinol (as shown in Fig. 8). These species act rapidly and non-selectively, breaking down even stable aromatic structures.

Simultaneously, O_3, a longer-lived oxidant, can directly oxidize certain intermediate compounds and acts as a precursor to $^{\bullet}OH$ generation. The prime oxidizing species is $^{\bullet}OH$ radical and, as shown in Fig. 8. Initially, $^{\bullet}OH$ radicals create nitro-catechol (II) when they react with PNP at the ortho position about the hydroxyl group. The subsequent hydroxylation of PNP produced an intermediate benzoquinone (VII). The nitro-catechol transforms into hydroxyquinol (VIII) after losing its nitro group. Then, both of the produced intermediates underwent oxidation to yield low molecular weight unsaturated carboxylic acids (but-2-enedioic acid (III) and saturated carboxylic acids (propanedioic acid (V) and oxalic acid (VI)). The other literature dealing with the degradation of PNP using plasma also reports a similar degradation species where degradation of PNP is dominated by $^{\bullet}OH$ radicals producing muconic acid, succinic acid, 2-oxomalonic acid, and 2-hydroxymalonic acid. Finally, these products of ring-opening reactions were further mineralized into inorganic molecules, e.g., CO_2, H_2O, NO_2^-, and NO_3^- (Zhao et al., 2022; Khourshidi et al., 2024; Farzinfar and Qaderi, 2022). Also, $^{\bullet}O_2^-$ radical quantified in the reaction medium and $HO_2^{\bullet}$ radicals can participate in redox cycling and act as reducing/oxidizing agents depending on the pH and solution chemistry. Under acidic plasma conditions, $HO_2^{\bullet}$ dominates and can react with organics or regenerate $^{\bullet}OH$ through secondary reactions, enhancing the radical pool. The synergy among these species creates a cascade effect: O_3 and $^{\bullet}O_2^-$ radical species extend the oxidative lifetime and reach of plasma treatment by generating $^{\bullet}OH$ radicals even after the plasma is turned

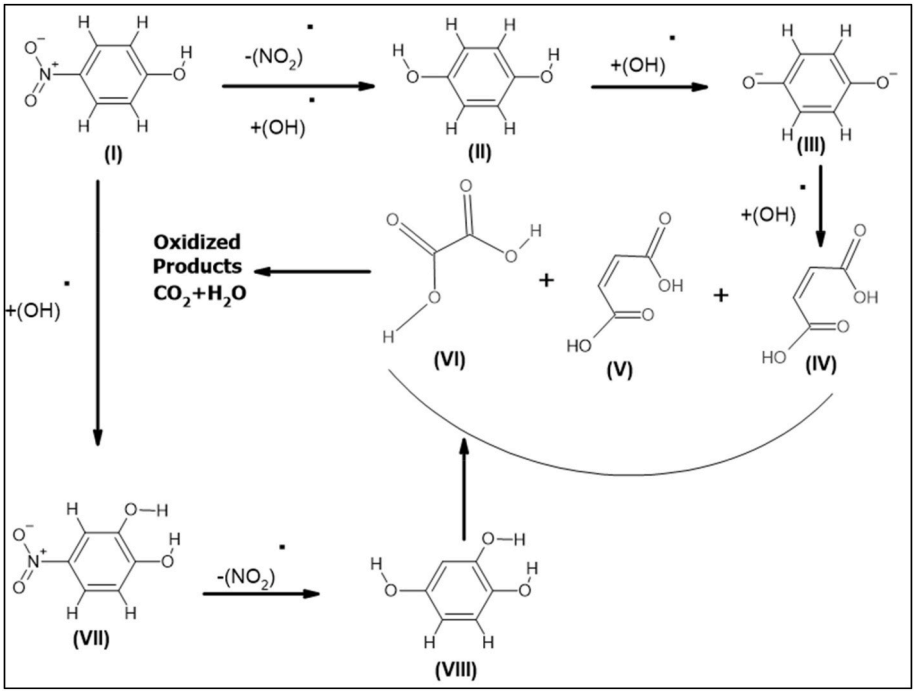

Fig. 8. A plausible mechanism proposed for PNP degradation. Adapted from reference (Yadav et al., 2023; Moctezuma et al., 2012).

off. This complex interplay ensures more complete degradation of pollutants, including intermediates, compared to what could be achieved by any single species alone. At optimal plasma power (18–22 W), the balance between generation and quenching of RONS is most favourable, enabling maximal degradation efficiency and energy yield. At higher powers, excessive heating leads to species quenching, especially of ●OH, thereby disrupting this synergistic balance and diminishing degradation efficiency.

This synergistic behaviour is essential for applying plasma in wastewater treatment, especially for complex pollutant mixtures, where multiple oxidation pathways must be simultaneously activated for effective remediation.

Table 2 represents the comparative study of available literature reports on plasma for PNP degradation. Various plasma combinations are employed for PNP degradation. The existing literature indicates that not all studies are compared using a single benchmark parameter. Our observed degradation aligns with existing research, demonstrating that with a shorter treatment time of 2 min and a power of 22 W, an energy yield of 14.4 g/kWh of PNP removal can be achieved. In this study, we observe a significant reduction in plasma treatment time compared to other studies. Concerning energy yield, the microwave atmospheric plasma jet employed by Zhao et al. (2021, 2022) shows the highest energy yield of 657 and 615 g/kWh, significantly higher than our obtained values of 14.4 g/kWh. The concentration of reactive species produced by the two techniques differs, and the heating of the reactor, which the authors have decreased through coolant circulation, could be the potential reason behind the observed efficiency. As seen from Tables 2 and in comparison to DBD plasma and corona discharge plasma, the values of energy yield are significantly superior. The energy yield and PNP conversion reported in the current study could be further enhanced by reducing the heat generated in the reactor by using a coolant circulating or increasing the gas feed flow rate and changing plasma mode to nanosecond pulse mode, which is the future scope of the work.

Table 2
Comparative analysis of PNP degradation through plasma.

Plasma type	[PNP] (ppm)	Conversion (%)	Plasma operating parameters		Reference
			Plasma power, energy yield	Treatment time (min)	
DBD Fe/Peroxy Sulphate	5	81.1	4.2 W, 0.2295 g/kWh	50	Shang et al. (2019)
Liquid pulse discharge Peroxydisulphate	100	90	Applied voltage 13 kV, 0.04 g/kWh	–	Shang et al. (2017)
Plasma Jet	100	55	43 mJ, 0.025 mgkJ^{-1}	5	Chen et al. (2019)
DBD $CoFe_2O_4$/MWNTs/sponge	10	98.5	30 V	40	Long et al. (2021)
Multi-tube parallel surface discharge plasma reactor	40	97	30 kV, 27.4 g/kWh	180	Wang et al. (2012)
Gliding Arc discharge	140	90	10 kV	120	Ferhat et al. (2017)
DBD	100	15	110 V	30	Wang et al. (2020)
Microwave atmospheric plasma jet	100	100	380 W, ~657 g/kWh	12	Zhao et al. (2021)
Microwave atmospheric pressure plasma	100	93.6	380 W, ~615 g/kWh	12	(Zhao et al., 2022)]
plasma jets, the mixed Argon jet	100	97.2	57.3 g/kWh	6	Acharya et al. (2024)
Corona discharge of needle-to-plate graphene-ZnO nanoparticles	30	93.6 %	Voltage 20 kV, frequency 50 Hz	30	(Guo et al., 2024)
DBD plasma O_3 circulation	50	94.4	16 kV,1.18 g/kWh	30	Khourshidi et al. (2024)
DBD plasma	15	93.6	13 kV	30	Farzinfar and Qaderi (2022)
DBD plasma	100	77	22 W, 14.4 g/kWh	2	Present study

3.2. Degradation of multiple organic pollutants

The reactor is tested for the degradation of multiple organic pollutants in a single treatment using plasma. For this purpose, a 20-ppm solution of each *benzene, toluene, and PNP* (totalling 60 ppm) is mixed to simulate a real-life elution situation. These organic compounds are chosen because they are commonly found in water and used in industry as solvents or precursors for synthesizing various products. Individual degradation studies of these organic pollutants have been conducted in multiple studies. However, degrading multiple organic contaminants in a single go is challenging and tedious.

Fig. 9 represents the percentage degradation of multiple organics in wastewater. At a power of 18 W, a maximum of 55 ± 5 % of total organics degradation in water is observed. The further increase in input power to 22 W organic removal decreases to 35 ± 5 %. At 30 W and 40 W input power, less than 30 ± 5 % of organic removal occurs. The plausible degradation mechanism of individual benzene and toluene adapted from literature is provided in the supplementary information file Figs. S7–S8 **ESI†**. It has been observed that complete COD removal is not achieved for the mixture of organic pollutants. This may be due to the many reactive intermediates that are formed and not mineralized. The detailed degradation mechanism of multiple pollutants is complicated and beyond the scope of current work. A similar trend is noted for energy yield. The degradation of organic pollutants from COD is found to be maximum at 18 W; at this power, the concentration of reactive species is also at its peak, resulting in an energy yield of 0.73 gCOD/kWh. However, further increases in plasma power decrease energy yield to 0.47 gCOD/kWh at 22 W. This reduction is attributed to a decline in the reactive species concentration, as discussed previously. The energy yield in the given system can be further enhanced by adjusting the operating conditions, such as circulating coolant and changing the plasma operating mode from continuous to pulse mode, which can reduce the heating effect in the reactor.

The multiple organics containing water are analysed for BOD (biochemical oxygen demand analysis). The BOD indicates the amount of oxygen available in the reaction mixture for microorganisms' degradation of organics in water. Fig. 10 shows untreated water (multiple pollutants) has a higher BOD value than distilled water. The higher BOD levels infer that more oxygen is required for pollutant degradation in biological species. The plasma treatment leads to a 2.5-fold lowering in BOD value at 18 W. The further increase in plasma power leads to a 2.7-fold lowering in BOD value at 22 W. The decrease indicates a lowering of water's organic toxicity after treatment and plasma's effectiveness in degrading multiple organic pollutants simultaneously. The biodegradability of the plasma-treated wastewater was assessed using the BOD/COD ratio at varying discharge powers (18, 22, 30, and 40 W), resulting in ratios of 0.055, 0.079, 0.109, and 0.084, respectively.

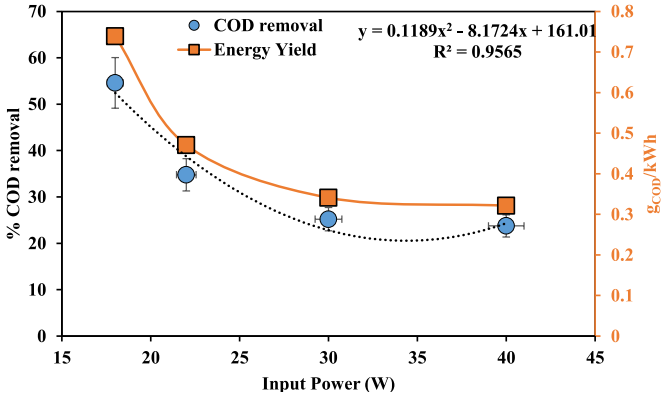

Fig. 9. Degradation of multiple organics in water at fixed plasma treatment time 2 min.

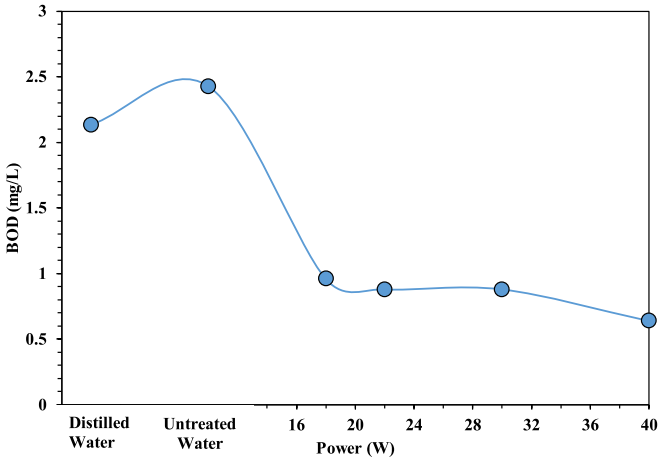

Fig. 10. The variation in BOD (biochemical oxygen demand) of water treated with plasma at a fixed treatment time of 2 min.

All values remained below the standard biodegradability threshold of 0.3, indicating limited biodegradability. The maximum biodegradability was observed at 30 W, suggesting optimal plasma conditions within our tested range. However, the persistence of refractory intermediates generated during plasma treatment highlights the importance of enhancing $^{\bullet}OH$ radicals' production. Our setup is limited due to excessive heating effects on reactor walls and the aqueous solution. Consequently, future strategies could include biological post-treatment or further optimization of plasma parameters (e.g., discharge duration, gas composition, power modulation) to improve the overall wastewater treatment efficacy.

The multiple organics containing water and post treatment water was used for evaluation of phytotoxicity using *Triticum aestivum* seeds as model. Table 3 presents the effect of plasma treatment on *Triticum aestivum* (wheat seeds). It is observed that the plasma treatment leads to enhanced seed germination compared to control water and multiple organic pollutants. On D_0+1 with water, 80 % germination is observed, whereas in the presence of numerous organic pollutants, 70 % germination is observed. Upon plasma ignition in the solution of multiple organic pollutants, the germination percentage is raised to 90 % at 18 W, which increases to 100 % germination at 22 W of input power. The increase in germination percentage is attributed to a lowering in organic toxicity and an added boost for germination *via* an increased concentration of NO_2^- and NO_3^- species in water, which counteracts abscisic acid and initiates germination. The abscisic acid controls seed dormancy. Similarly, the shoot length of wheat seeds added with plasma-treated multiple organic pollutants is higher than the untreated sample. This is attributed to nitrates and nitrites in plasma-treated water samples, which act as chemical fertilizers Fig. S9 **ESI†**.

Plasma treatment lowered water's phytotoxicity, as evidenced by previous studies. Apart from the organics, pathogens can also affect

Table 3
Effect of plasma treatment on percentage germination and shoot length.

Seed samples	Germination % (D_0 + 1)	Shoot Length (cm)			
		(D_0 + 1)	(D_0 + 2)	(D_0 + 3)	(D_0 + 4)
Control (water)	80	0.75	1.75	5.05	6.55
Control (Multiple organic Pollutants)	70	0.5	1.5	4.65	7.2
18 W	90	0.7	1.7	5.6	6.75
22 W	100	0.55	1.65	4.9	6.9
30 W	60	0.45	1.4	4.3	6.5
40 W	70	0.5	1.5	4.1	5

D_0 = Day of treatment, Values are expressed as mean, n = 3.

water quality, making it unfit for usage. Thus, a bacterial toxicity study to explore the inhibition of the growth of *E. coli* as a model pathogen strain with plasma is evaluated by varying plasma input power and treatment time. Fig. 11 depicts the impact of plasma input power at a constant plasma treatment time of 2 min. It's observed that when plasma power increased from 18 to 40 W with a fixed treatment time of 2 min, growth inhibition of *E. coli* colonies increased. Table 4 depicts percentage growth inhibition as a function of plasma input power. At 18 W of plasma power, 14.38 ± 1.63 % growth inhibition is observed. The growth inhibition increases to 28.57 ± 1.24 % at 26 W, a 2-fold increase compared to 18 W plasma power. The increase in plasma power to 30 W led to a 1.68-fold increase in inhibition of *E. coli* colonies. Further, at 40 W, 74.13 ± 1.69 % inhibition of *E. coli* colonies was obtained.

The multiple pollutant containing water and post treatment water was used for evaluation of phytotoxicity using *Triticum aestivum* seeds as model. Fig. 12 demonstrates the influence of plasma treatment on growth inhibition at a fixed power of 22 W. The 1-min plasma treatment resulted in 10.67 ± 1.25 % growth inhibition *of E. coli*. An extended duration of plasma treatment resulted in further growth inhibition. It can be observed through Table 5 compared to the control, the plasma treatment of 3 min led to ≈50 % inhibition of *E. coli's* growth. Treatment lasting 4 and 5 min with plasma resulted in 67.78 ± 0.82 % and 98.09 ± 1.25 % growth inhibition of *E. coli*, respectively. Furthermore, after 10 min, no growth of *E. coli* was observed, indicating complete inhibition of the bacterial cells.

This trend differs from pollutant degradation, where increased plasma input power and treatment time result in lower degradation of pollutants. In contrast, the inactivation of *E.coli* bacterial colonies increases with both plasma input power and treatment time. This can be attributed to selective species, namely $^{\bullet}OH$, which plays an effective role in pollutant degradation due to its high oxidation potential. Conversely, all reactive oxygen and nitrogen species contribute to the inactivation of bacterial colonies.

To statistically validate the role of plasma in microbial inhibition and its contribution to BOD reduction, a two-way ANOVA with replication was performed using bacterial inactivation data across five plasma power levels (0, 18, 26, 30, and 40 W), each with three replicates. Notably, the interaction term Power × BOD was found to be highly significant ($F = 437.71$, $p < 0.0001$), indicating a strong combined effect of plasma power and organic load (BOD) on microbial inactivation efficiency. Detailed ANOVA results are provided in Table 1 **ESI†**.

The improvement in seed germination and shoot length observed with plasma-treated water, especially at 18 W and 22 W input power, indicates a notable decrease in phytotoxicity. This suggests that DBD plasma treatment effectively diminishes the toxicity of organic pollutants in water, making the treated water more suitable for agricultural reuse. The enhanced seed germination rate may also stem from plasma-generated nitrate and nitrite species, which are known to promote germination by counteracting abscisic acid and boosting seed metabolic activity.

Moreover, the reduction of *E. coli* noted in the bacterial inhibition assay underscores the antimicrobial effectiveness of the plasma treatment. This is particularly significant for practical wastewater treatment applications, where microbial contamination poses health hazards.

Table 4
Inhibition of growth of *E. coli* (%) at different power for 2 min.

Power (W)	% growth inhibition
Control (Untreated)	0
18	14.38 ± 1.63
26	28.57 ± 1.24
30	48.16 ± 0.81
40	74.13 ± 1.69

Values are expressed as mean ± SD, n = 3.

Achieving complete bacterial inhibition at higher plasma doses demonstrates the potential of this method for controlling pathogens while degrading pollutants. These findings indicate that the DBD plasma system provides a dual advantage—chemical detoxification and microbial disinfection—crucial for effective water purification and safe agricultural or environmental reuse. Overall, the improved seed germination and complete bacterial inhibition suggest reduced phytotoxicity and effective microbial disinfection, indicating potential reuse in agricultural and sanitation contexts. However, low-biodegradability intermediates and a lack of long-term ecological data highlight the need for complementary treatments or monitoring before large-scale deployment.

4. Conclusion

This study examines a DBD reactor for removing P-nitrophenol (PNP) and other pollutants from water. About 70 % degradation of 10 ppm PNP occurs at 18 W in 2 min, with energy yield of 1.57 mg/kWh; both degradation and yield decline with higher power. Increasing microdischarge channels heat walls, reducing necessary radicals. The main reactive species are O_3, $^{\bullet}OH$, and $^{\bullet}O_2^-$, which oxidize PNP. Longer treatment times decrease degradation. Trends align with plasma species concentration; O_3 increases with power but decreases with time, while $^{\bullet}OH$ and $^{\bullet}O_2^-$ concentrations drop due to quenching. The plasma efficiently removes multiple organic pollutants (benzene, toluene, PNP) at optimal conditions (18 W, 2 min), achieving 55 % degradation and 0.73 gCOD/kWh energy yield. COD analysis supports this degradation; BOD, phytotoxicity, and antimicrobial tests show reduced organic matter. Plasma-treated water improves wheat seed germination due to beneficial NO_2^- and NO_3^- species. Increased energy and treatment time inhibit *E. coli* growth. A two-way ANOVA indicates significant effects of plasma power and BOD on inhibition ($p < 0.0001$). DBD plasma's practicality is confirmed by enhanced germination and microbial inactivation, reducing toxicity for reuse in irrigation or discharge. For a single pollutant at 100 ppm, 14.4 g/kWh energy yield is achieved at 22 W in 2 min, while 0.73 g/kWh is noted for multiple pollutants. Although PNP efficiency is lower than some high-power systems, our method offers advantages like ambient operation, no additional chemicals, and compact scalability. Significant degradation without secondary waste positions it as a clean alternative to conventional processes. This work verifies $^{\bullet}OH$'s role in degradation and microbial inactivation, but the mechanism is hypothetical due to undetected intermediates. Future studies should use sophisticated techniques to clarify degradation pathways and interactions in complex mixture interaction effects.

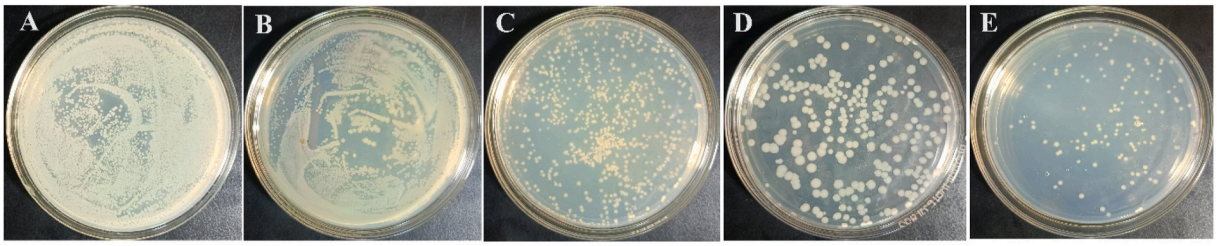

Fig. 11. Growth inhibition of *E. coli* at different input power for 2 min (A) Control (Untreated), (B) 18 W, (C) 26 W, (D) 30 W, (E) 40 W.

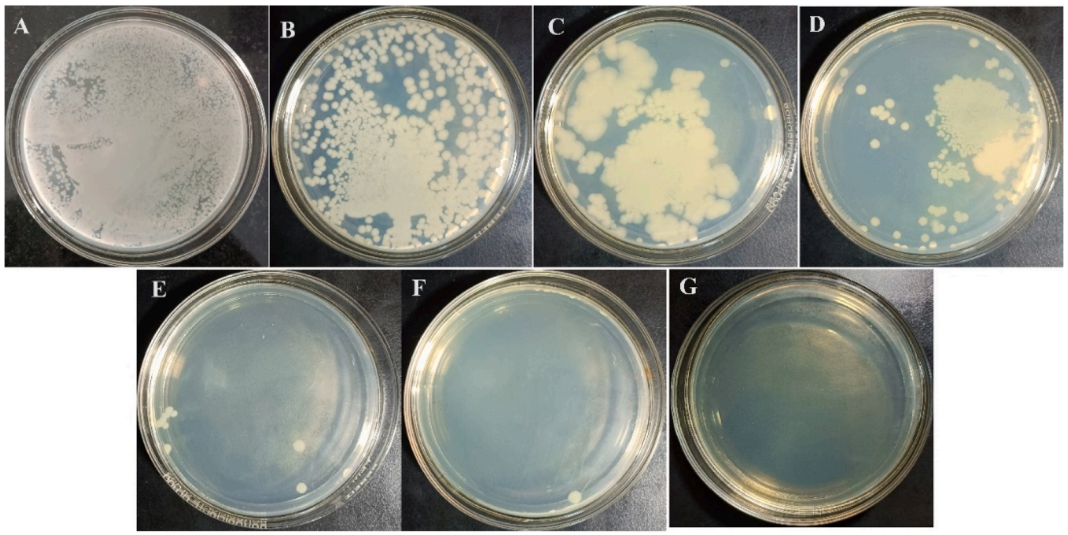

Fig. 12. Growth inhibition of *E. coli* at different time intervals at the fixed plasma power of 22 W: (A) 0 min (control), (B) 1 min, (C) 2 min, (D) 3 min, (E) 4 min, (F) 5 min, (G) 10 min.

Table 5
Inhibition of growth of *E. coli* (%) at various treatment times at a plasma input power of 22 W.

Time interval (in minutes)	% growth inhibition
0 (control or untreated)	0
1	10.67 ± 1.25
2	26.57 ± 1.25
3	48.26 ± 2.05
4	67.78 ± 0.82
5	98.09 ± 1.25
10	100

Values are expressed as mean ± SD, n = 3.

Results highlight the system's dual-function capability and robust performance. The enhanced efficiency can be achieved by reducing energy losses and thermal effects while improving electron utilization. Optimizing dielectric materials, gas flow, and catalytic surfaces may extend radical lifetimes. This study confirms DBD plasma's potential for degrading organic pollutants and microbial contaminants with a small sample volume. Thus, paving the way for further development of setup for improving pollutant removal efficiency.

CRediT authorship contribution statement

Vaishnavi Gaude Agadyekar: Investigation, Data curation. **Eshita Kakodkar:** Investigation, Formal analysis, Data curation. **Delicia A. Barretto:** Writing – review & editing, Writing – original draft, Resources, Methodology, Investigation, Formal analysis, Data curation. **Ruggero Barni:** Writing – review & editing, Conceptualization. **Claudia Riccardi:** Writing – review & editing. **Nitesh Joshi:** Writing – review & editing, Writing – original draft, Visualization, Validation, Supervision, Resources, Project administration, Methodology, Investigation, Formal analysis, Data curation, Conceptualization.

Declaration of competing interest

The authors declare that they have no known competing financial interests or personal relationships that could have appeared to influence the work reported in this paper.

Acknowledgement

Nitesh Joshi and Delicia Barretto acknowledge the UGC-SAP and DST-FIST for supporting instrumental facilities at the School of Chemical Science at Goa University. This work was also funded by the National Plan for NRRP Complementary Investments (PNC, established with the decree-law 6 May 2021, n. 59, converted by law n. 101 of 2021) in the call for the funding of research initiatives for technologies and innovative trajectories in the health and care sectors (Directorial Decree n. 931 of 6 June 2022)—project n. PNC0000003—Advanced Technologies for Human-centrEd Medicine (project acronym: ANTHEM). This work reflects only the authors' views and opinions; neither the Ministry for University and Research nor the European Commission can be considered responsible for them.

Appendix A. Supplementary data

Supplementary data to this article can be found online at https://doi.org/10.1016/j.clet.2025.101042.

Data availability

Data will be made available on request.

References

Acharya, T.R., Lamichhane, P., Jaiswal, A., Kaushik, N., Kaushik, N.K., Choi, E.H., 2024. Evaluation of degradation efficacy and toxicity mitigation for 4-nitrophenol using argon and air-mixed argon plasma jets. Chemosphere 358, 142211. https://doi.org/10.1016/j.chemosphere.2024.142211.

Anjum, H., Johari, K., Gnanasundaram, N., Ganesapillai, M., Arunagiri, A., Regupathi, I., Thanabalan, M., 2019. A review on adsorptive removal of oil pollutants (BTEX) from wastewater using carbon nanotubes. J. Mol. Liq. 277, 1005–1025. https://doi.org/10.1016/j.molliq.2018.10.105.

APHA, 2017. Standard Methods for the Examination of Water and Wastewater, 23rd ed. American Public Health Association, American Water Works Association, Water Environment Federation, Washington, D.C.

Archer, T.E., 1975. Dissipation of parathion and related compounds from field-sprayed lettuce. J. Agric. Food Chem. 23 (5), 858–860. https://doi.org/10.1021/jf60201a025.

Bedeaux, D., Ortiz de Zárate, J.M., Pagonabarraga, I., Sengers, J.V., Kjelstrup, S., 2011. Concentration fluctuations in non-isothermal reaction-diffusion systems. II. The nonlinear case. J. Chem. Phys. 135, 124904. https://doi.org/10.1063/1.3640010.

Bustillo-Lecompte, C.F., Kakar, D., Mehrvar, M., 2018. Photochemical treatment of benzene, toluene, ethylbenzene, and xylenes (BTEX) in aqueous solutions using advanced oxidation processes: towards a cleaner production in the petroleum refining and petrochemical industries. J. Clean. Prod. 186, 609–617. https://doi.org/10.1016/j.jclepro.2018.03.135.

Chandana, L., Ray, D., Subrahmanyam, C., 2022. Physicochemical process of non-thermal plasma at gas–liquid interface and synergistic effect of plasma with catalyst. Curr. Appl. Phys. 36, 16–26. https://doi.org/10.1016/j.cap.2022.01.006.

Chandana, L., Subrahmanyam, C., 2017. Non-thermal discharge plasma promoted redox transformation of arsenic (III) and chromium (VI) in an aqueous medium. Chem. Eng. J. 329, 211–219. https://doi.org/10.1016/j.cej.2017.05.114.

Chemical Marketing Reporter, 1990. Chemical Profile p-Nitrophenol. Schnell Pub Co, New York, NY.

Chen, B., Zhu, C., Chen, L., Fei, J., Gao, Y., Wen, W., Ren, Z., 2014. Atmospheric pressure plasma jet in organic solution: Spectra, degradation effects of solution flow rate and initial pH value. Plasma Sci. Technol. 16, 1126–1132. https://doi.org/10.1088/1009-0630/16/12/08.

Chen, B., Zhu, C., Fei, J., He, X., Yin, C., Wang, Y., Chen, L., 2016. Yield of ozone, nitrite nitrogen and hydrogen peroxide versus discharge parameter using APPJ under water. Plasma Sci. Technol. 18, 278. https://doi.org/10.1088/1009-0630/18/3/11.

Chen, B., Zhu, C., Fei, J., Jiang, Y., Yin, C., Su, W., Chen, Y., 2019. Reaction kinetics of phenols and p-nitrophenols in flowing aerated aqueous solutions generated by a discharge plasma jet. J. Hazard. Mater. 363, 55–63. https://doi.org/10.1016/j.jhazmat.2018.09.051.

Eisenberg, G., 1943. Colorimetric determination of hydrogen peroxide. Ind. Eng. Chem. Anal. Ed. 15, 327–328. https://doi.org/10.1021/i560117a011.

El-Hagrasy, A.M.A., et al., 2025. Investigating the general effects of different types of toluene exposure on the health of workers: an integrative review of the literature. BMJ Public Health 3, 1. https://doi.org/10.1136/bmjph-2024-001046.

Farzinfar, B., Qaderi, F., 2022. Synergistic degradation of aqueous p-nitrophenol using DBD plasma combined with ZnO photocatalyst. Process Saf. Environ. Prot. 168, 907–917. https://doi.org/10.1016/j.psep.2022.10.060.

Ferhat, M.F., et al., 2017. Conception of a novel spray tower plasma-reactor in a spatial post-discharge configuration: pollutants remote treatment. J. Hazard. Mater. 321, 661–671. https://doi.org/10.1016/j.jhazmat.2016.09.052.

Golkowski, M., et al., 2012. Hydrogen-peroxide-enhanced nonthermal plasma effluent for biomedical applications. IEEE Trans. Plasma Sci. 40, 1984–1991. https://doi.org/10.1109/tps.2012.2200910.

Goto, H., et al., 2004. Quantitative analysis of superoxide ion and hydrogen peroxide produced from molecular oxygen on photoirradiated TiO_2 particles. J. Catal. 225, 223–229. https://doi.org/10.1016/j.jcat.2004.04.001.

Graedel, T.E., McGill, R., 1986. Degradation of materials in the atmosphere. Environ. Sci. Technol. 20 (11), 1093–1100. https://doi.org/10.1021/es00153a003.

Gu, L., Zhang, X., Lei, L., 2008. Degradation of aqueous p-nitrophenol by ozonation integrated with activated carbon. Ind. Eng. Chem. Res. 47 (18), 6809–6815. https://doi.org/10.1021/ie071584h.

Guo, H., Yang, H., Huang, J., Tong, J., Liu, X., Wang, Y., Han, J., 2022. Theoretical and experimental insight into plasma-catalytic degradation of aqueous p-nitrophenol with graphene-ZnO nanoparticles. Sep. Purif. Technol. 295, 121362. https://doi.org/10.1016/j.seppur.2022.121362.

Howard, P.H., Michalenko, E.M., Jarvis, W.F., Basu, D.K., Sage, G.W., Meylan, W.M., Gray, D.A., 2017. Handbook of Environmental Fate and Exposure Data: for Organic Chemicals. Routledge. https://doi.org/10.1201/9780203719305.

Joshi, N., Loganathan, S., 2023. *In situ modification of CuO–Fe_2O3 by nonthermal plasma: insights into the CO_2-to-CH_3OH hydrogenation reaction*. ACS Omega 8, 13410–13420. https://doi.org/10.1021/acsomega.3c00915.

Joshi, N., Loganathan, S., 2024. Cold plasma techniques for sustainable material synthesis and climate change mitigation: a review. Catalysts 14, 802. https://doi.org/10.3390/catal14110802.

Joshi, N., Sivachandiran, L., Assadi, A.A., 2022. *Perspectives in advance technologies/strategies for combating rising CO_2 levels in the atmosphere via CO_2 utilisation: a review*. IOP Conf. Ser. Earth Environ. Sci. 1100, 012020. https://doi.org/10.1088/1755-1315/1100/1/012020.

Keith, L., Telliard, W., 1979. ES&T special report: priority pollutants: a perspective view. Environ. Sci. Technol. 13 (4), 416–423. https://doi.org/10.1021/es60152a601.

Khourshidi, A., Ajam, F., Rabieian, M., Taghavijeloudar, M., 2024. Efficient degradation of p-nitrophenol from water by enhancing dielectric barrier discharge (DBD) plasma through ozone circulation: optimization, kinetics and mechanism. Chemosphere 349, 142749. https://doi.org/10.1016/j.chemosphere.2024.142749.

Koshlyakov, P.V., Barkova, D.A., Gerasimov, I.E., Chesnokov, E.N., Zhang, X., Krasnoperov, L.N., 2021. Kinetics of the gas-phase reaction of hydroxyl radicals with trimethyl phosphate over the 273–837 K temperature range. RSC Adv. 11, 14121–14131. https://doi.org/10.1039/d1ra00911g.

Kulkarni, M., Chaudhari, A., 2007. Microbial remediation of nitro-aromatic compounds: an overview. J. Environ. Manag. 85 (2), 496–512. https://doi.org/10.1016/j.jenvman.2007.06.009.

Lhotský, O., Krákorová, E., Mašín, P., Žebrák, R., Linhartová, L., Křesinová, Z., Cajthaml, T., 2017. *Pharmaceuticals, benzene, toluene and chlorobenzene removal from contaminated groundwater by combined UV/H_2O_2 photo-oxidation and aeration*. Water Res. 120, 245–255. https://doi.org/10.1016/j.watres.2017.04.076.

Lewis, R.A., 2016. Hawley's Condensed Chemical Dictionary. John Wiley & Sons.

Li, R., Liu, Y., Sun, Y., Zhang, W., Mu, R., Li, X., Ognier, S., 2015. Degradation of p-nitrophenol in soil by dielectric barrier discharge plasma. Water Air Soil Pollut. 226, 436. https://doi.org/10.1007/s11270-015-2675-0.

Long, Y., Nie, J., Yuan, C., Ma, H., Chen, Y., Cong, Y., Zhang, Y., 2021. *Preparation of $CoFe_2O_4$/MWNTs/sponge electrode to enhance dielectric barrier plasma discharge for degradation of phenylic pollutants and Cr(VI) reduction*. Appl. Catal. B Environ. 283, 119604. https://doi.org/10.1016/j.apcatb.2020.119604.

Loprieno, N., 1975. International agency for research on cancer (IARC) monographs on the evaluation of carcinogenic risk of chemicals to man: relevance of data on mutagenicity. Mutat. Res. 31, 210.

Lunov, O., Zablotskii, V., Churpita, O., Jäger, A., Polívka, L., Syková, E., Kubinová, Š., 2016. The interplay between biological and physical scenarios of bacterial death induced by non-thermal plasma. Biomaterials 82, 71–83. https://doi.org/10.1016/j.biomaterials.2015.12.027.

Masumoto, H., Kurisu, F., Kasuga, I., Furumai, H., 2014. Benzene and toluene biodegradation potential in methanogenic cultures established by feeding benzene, toluene and their mixture. J. Water Environ. Technol. 12, 77–86. https://doi.org/10.2965/jwet.2014.77.

Mcguire, D., Jakhete, S., 2012. Apparatus for treating fluid. US Patent WO2012171006A1 filed 11 June 2012, issued 13 December 2012.

Meiyazhagan, S., Yugeswaran, S., Ananthapadmanabhan, P.V., Suresh, K., 2020. Process and kinetics of dye degradation using microplasma and its feasibility in textile effluent detoxification. J. Water Process Eng. 37, 101519. https://doi.org/10.1016/j.jwpe.2020.101519.

Mhapsekar, S., Kalangutkar, N., Joshi, N., 2025. Microplastic contamination and ecological risk in a riverine system: a case study from the valvanti river, Goa, India. Environ. Monit. Assess. 197, 706. https://doi.org/10.1007/s10661-025-14168-2.

Moctezuma, E., Leyva, E., Aguilar, C.A., Luna, R.A., Montalvo, C., 2012. Photocatalytic degradation of paracetamol: intermediates and total reaction mechanism. J. Hazard. Mater. 243, 130–138. https://doi.org/10.1016/j.jhazmat.2012.10.010.

Nojima, K., Kawaguchi, A., Ohya, T., Kanno, S., Hirobe, M., 1983. Studies on photochemical reaction of air pollutants. X. Identification of nitrophenols in suspended particulates. Chem. Pharm. Bull. 31 (3), 1047–1051. https://doi.org/10.1248/cpb.31.1047.

Oba, Y., Watanabe, N., Kouchi, A., Hama, T., Pirronello, V., 2011. *Experimental studies of surface reactions among OH radicals that yield H_2O and CO_2 at 40–60 K*. Phys. Chem. Chem. Phys. 13, 15792–15797. https://doi.org/10.1039/c1cp20596j.

Othman, I., Haija, M.A., Ismail, I., Zain, J.H., Banat, F., 2019. *Preparation and catalytic performance of $CuFe_2O_4$ nanoparticles supported on reduced graphene oxide ($CuFe_2O_4$/rGO) for phenol degradation*. Mater. Chem. Phys. 238, 121931. https://doi.org/10.1016/j.matchemphys.2019.121931.

Parrino, F., Livraghi, S., Giamello, E., Ceccato, R., Palmisano, L., 2020. *Role of hydroxyl, superoxide, and nitrate radicals on the fate of bromide ions in photocatalytic TiO_2 suspensions*. ACS Catal. 10, 7922–7931. https://doi.org/10.1021/acscatal.0c02010.

Penetrante, B.M., Hsiao, M.C., Bardsley, J.N., Merritt, B.T., Vogtlin, G.E., Kuthi, A., Bayless, J.R., 1997. Identification of mechanisms for decomposition of air pollutants by non-thermal plasma processing. Plasma Sources Sci. Technol. 6, 251–259. https://doi.org/10.1088/0963-0252/6/3/002.

Piferi, C., Barni, R., Roman, H.E., Riccardi, C., 2021. Current filaments in asymmetric surface dielectric barrier discharge. Appl. Sci. 11, 2079. https://doi.org/10.3390/app11052079.

Piferi, C., Riccardi, C., 2022. A study on propane depletion by surface dielectric barrier discharges. Clean. Eng. Technol. 8, 100486. https://doi.org/10.1016/j.clet.2022.100486.

Pierotti, G., Piferi, C., Popoli, A., Cavedon, M., Cristofolini, A., Martines, E., Riccardi, C., 2023. A novel two-stage kinetic model for surface DBD simulations in air. Plasma Sources Sci. Technol. 32, 064005. https://doi.org/10.1088/1361-6595/acdea2.

Sahni, M., Locke, B.R., 2006. Quantification of hydroxyl radicals produced in aqueous phase pulsed electrical discharge reactors. Ind. Eng. Chem. Res. 45, 5819–5825. https://doi.org/10.1021/ie0601504.

Shang, K., Hao, W., Jie, L., Na, L.U., Jiang, N., Yan, W.U., 2017. Activation of peroxydisulphate by gas–liquid pulsed discharge plasma to enhance the degradation of p-nitrophenol. Plasma Sci. Technol. 19, 064017. https://doi.org/10.1088/2058-6272/aa6616.

Shang, K., Li, W., Wang, X., Lu, N., Jiang, N., Li, J., Wu, Y., 2019. *Degradation of p-nitrophenol by DBD plasma/Fe^{2+}/persulphate oxidation process*. Sep. Purif. Technol. 218, 106–112. https://doi.org/10.1016/j.seppur.2019.02.046.

Tas, M.A., Van Hardeveld, R., Van Veldhuizen, E.M., 1997. Reactions of NO in a positive streamer Corona plasma. Plasma Chem. Plasma Process. 17, 371–391. https://doi.org/10.1023/A:1021818313047.

Tremp, J., Mattrel, P., Fingler, S., Giger, W., 1993. Phenols and nitrophenols as tropospheric pollutants: emissions from automobile exhausts and phase transfer in the atmosphere. Water Air Soil Pollut. 68 (1), 113–123. https://doi.org/10.1007/BF00479396.

Wang, J., Li, L., Cao, H., Yang, C., Guo, Z., Shi, Y., Xie, Y., 2020. Degradation of phenolic compounds by dielectric barrier plasma: process optimization and influence of phenol substituents. Chem. Eng. J. 385, 123732. https://doi.org/10.1016/j.cej.2019.123732.

Wang, T., Qu, G., Ren, J., Sun, Q., Liang, D., Hu, S., 2016. Organic acids enhanced decoloration of azo dye in gas phase surface discharge plasma system. J. Hazard. Mater. 302, 65–71. https://doi.org/10.1016/j.jhazmat.2015.09.051.

Wang, T., Qu, G., Sun, Q., Liang, D., Hu, S., 2015. Evaluation of the potential of p-nitrophenol degradation in dredged sediment by pulsed discharge plasma. Water Res. 84, 18–24. https://doi.org/10.1016/j.watres.2015.07.022.

Wang, T.C., Lu, N., An, J.T., Zhao, Y., Li, J., Wu, Y., 2012. Multi-tube parallel surface discharge plasma reactor for wastewater treatment. Sep. Purif. Technol. 100, 9–14. https://doi.org/10.1016/j.seppur.2012.08.014.

Yadav, V., Verma, P., Negi, H., Singh, R.K., Saini, V.K., 2023. *Efficient degradation of 4-nitrophenol using VO(TPP) impregnated TiO_2 photocatalyst: insight into kinetics and mechanism*. J. Mater. Res. 38, 237–247. https://doi.org/10.1557/s43578-022-00856-z.

Yao, Y.X., Li, H.B., Liu, J.Y., Tan, X.L., Yu, J.G., Peng, Z.G., 2014. Removal and adsorption of p-nitrophenol from aqueous solutions using carbon nanotubes and their composites. J. Nanomater. 2014, 642986. https://doi.org/10.1155/2014/571745.

Yukinori, S., David, B., Hungwen, C., 2012. Plasma chemistry model of surface microdischarge in humid air and dynamics of reactive neutral species. J. Phys. D Appl. Phys. 45, 425201. https://doi.org/10.1088/0022-3727/45/42/425201.

Zeng, L., Gong, J., Dan, J., Li, S., Zhang, J., Pu, W., Yang, C., 2019. Novel visible light enhanced pyrite-fenton system toward ultrarapid oxidation of p-nitrophenol: catalytic activity, characterization and mechanism. Chemosphere 228, 232–240. https://doi.org/10.1016/j.chemosphere.2019.04.103.

Zhao, C., Xue, L., Shi, H., Chen, W., Zhong, Y., Zhang, Y., Huang, K., 2022. Simultaneous degradation of p-nitrophenol and reduction of Cr(VI) in one step using microwave atmospheric pressure plasma. Water Res. 212, 118124. https://doi.org/10.1016/j.watres.2022.118124.

Zhao, C., Xue, L., Zhou, Y., Zhang, Y., Huang, K., 2021. A microwave atmospheric plasma strategy for fast and efficient degradation of aqueous p-nitrophenol. J. Hazard. Mater. 409, 124473. https://doi.org/10.1016/j.jhazmat.2020.124473.